Stochastic transition in the unequal-mass Toda lattice*

Giulio Casati
Istituto di Fisica, Via Celoria 16, 20133 Milano, Italy

Joseph Ford
School of Physics, Georgia Institute of Technology, Atlanta, Georgia 30332

(Received 5 June 1975)

In this paper, the results of various computer experiments performed on the two-particle, unequal-mass Toda lattice are discussed. These experiments indicate that this system exhibits a transition from near-integrable to macroscopically observable stochastic behavior at a critical value of the total energy E_c which depends on the mass ratio of the two particles (m_2/m_1). This transition appears to occur for every mass ratio in the open interval $0 < m_2/m_1 < 1$. Details of trajectory behavior at selected energies and mass ratios are exposed through presentation of a number of Poincaré surfaces of section. The transition discussed herein will likely prove to be significant for both mathematics and physics.

I. INTRODUCTION

Both computer experiment[1] and rigorous mathematical theory[2] show the Toda lattice[3] to be an integrable[4] system. In view of the physical[5] and mathematical[6] significance of the Toda lattice, it is of interest to determine the extent to which integrable or near-integrable behavior persists under perturbations of the Toda Hamiltonian. Now certainly almost every perturbation of the Toda Hamiltonian, no matter how small, would yield a nonintegrable system.[7] However, the Kolmogorov-Arnold-Moser (KAM) theorem[8] ensures that, for sufficiently small change, the nonintegrable Hamiltonian will remain at least near integrable in the sense that most trajectories will continue to lie on smooth integral surfaces. Moreover, various computer experiments[9,10] show that the KAM-type near-integrable behavior can persist far beyond the small perturbation range assumed by the KAM theorem. Nonetheless, when a nonintegrable perturbation becomes sufficiently large, many (if not most) system trajectories are wildly erratic, covering much of the energy surface in a seemingly ergodic and mixing fashion.[11] In this paper, we seek to determine via computer experiments the type of behavior which occurs as the perturbation parameters vary.

In the computer experiments to be discussed here, we chose to perturb the Toda Hamiltonian by introducing unequal masses into the lattice. This is a somewhat natural perturbation in the sense that isotopic mass impurities do occur in nature; in addition, this modification permits easy control of the perturbation strength. Although we have studied the effect on integrability of introducing mass defects into the many-particle Toda lattice (to be reported elsewhere), the experiments to be discussed here treat only the two-particle unequal-mass system using fixed-end boundary conditions. In particular, the Hamiltonian system we investigate here may be written

$$H = \tfrac{1}{2}\left[p_1^2/m_1 + p_2^2/m_2\right] + e^{-q_1} + e^{-(q_2-q_1)} + e^{q_2} - 3 \,, \tag{1}$$

where p_1, p_2 are particle momenta, q_1, q_2 are particle displacements from equilibrium, and m_1, m_2 are the particle masses. This two-particle system has several virtues. First, it displays all the essential properties of the many-particle system; second, it allows study of the complete range of mass ratio m_2/m_1 from zero to unity; third, it permits use of an easily viewed, graphical survey of a complete energy hypersurface via a Poincaré surface of section[12]; and last, it has only two relevant perturbation parameters, namely, the total energy E and the mass ratio m_2/m_1. Although the size of the total energy E does not appear to determine integrability or its lack for this system, we nonetheless choose to regard E as a perturbation parameter because, regardless of mass ratio m_2/m_1, for sufficiently small E most system trajectories lie on integral surfaces close to those of the integrable harmonic-oscillator system obtained by expanding the exponentials in Hamiltonian (1) and retaining only terms through quadratic order. Increasing the energy E at fixed m_2/m_1 thus allows the possibility of converting the behavior of most system trajectories from near-integrable to wildly erratic.

In Sec. II, we first show that a transition (the so-called stochastic[13] transition) from near-integrable to wildly erratic, obviously nonintegrable, behavior appears to occur for every mass ratio, except for the endpoint values $m_2/m_1 = 0$ or 1 which, of course, yield precisely integrable Hamiltonians. We then present a set of Poincaré surfaces of section showing the detailed behavior of trajectories

as the mass ratio or the energy varies. Finally in Sec. III, we present our conclusions.

II. RESULTS OF COMPUTER EXPERIMENTS

In phase-space regions where the unequal-mass Toda Hamiltonian yields near-integrable behavior, the separation distance D, given by

$$D=[(p_1'-p_1)^2+(p_2'-p_2)^2+(q_1'-q_1)^2+(q_2'-q_2)^2]^{1/2}, \tag{2}$$

between members of an initially close trajectory-pair, grows linearly[14] with time; a typical case is shown in Fig. 1. On the other hand, wildly erratic (stochastic) trajectories separate exponentially[14] from their initially close neighbors; Fig. 2 shows a typical example. For each mass ratio m_2/m_1 that we investigated (excluding the endpoints zero and unity), we always found a transition from linear to exponential separation as we increased the total energy E. In Fig. 3, we graph an empirically determined curve of E_c, an approximate value for the critical energy at which the linear to exponential transition occurs, versus mass ratio m_2/m_1. The curve in Fig. 3 should for several reasons be regarded as only a very crude estimate of E_c. First, as detected by the computer, the transition from linear to exponential separation occurs quite

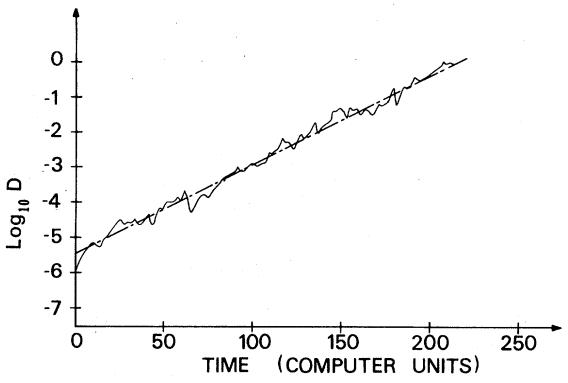

FIG. 2. Graph showing a typical curve of exponential growth in separation distance. Here, a curve of $\log_{10}D$ vs time is plotted, and one notes that D has increased by six powers of ten during the same time interval shown in Fig. 1. As in Fig. 1, $m_2/m_1=0.54$ and $E=7$; but here initially $q_1=-0.66$, $q_2=0$, $p_1=-0.037$, and $p_2=4.92$. The initial condition for the second trajectory differed from the first only in that $q_1'=q_1+10^{-6}$. This trajectory pair was initiated in a stochastic region of Fig. 8. Comparing Figs. 1 and 2, whether or not one accepts the labels "linear" or "exponential", one cannot ignore the strikingly different growth rates of D in the two figures.

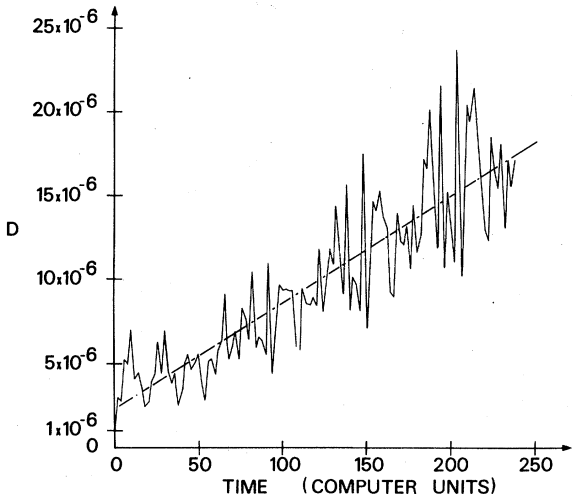

FIG. 1. Graph showing typical linear (on the average) growth of separation distance $D=[(p_1'-p_1)^2+(p_2'-p_2)^2+(q_1'-q_1)^2+(q_2'-q_2)^2]^{1/2}$ vs time, measured in differential equation seconds. D is the separation distance between two initially close trajectories. Here $m_2/m_1=0.54$, and $E=7$. One trajectory was initiated at $q_1=1.74$, $q_2=0$, $p_1=1.50$, and $p_2=2.72$; initial conditions for the second trajectory were obtained from the first by changing only q_1, setting $q_1'=q_1+10^{-6}$. This trajectory pair was initiated in a near-integrable region of Fig. 8.

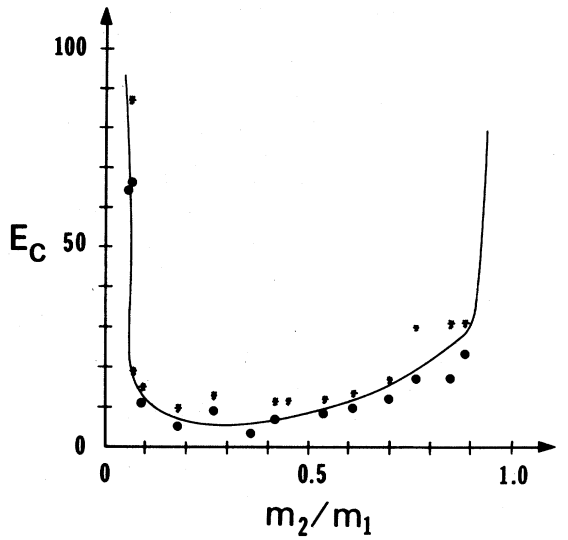

FIG. 3. Curve of transition energy E_c vs mass ratio m_2/m_1, where E_c is the approximate energy at which the computer detects a transition from linear to exponential growth of D. Dots denote linear growth, while asterisks denote exponential growth. For the particular trajectory pair we chose to integrate, the curve rises very steeply for mass ratios greater than 0.9 and less than 0.07. Regardless of trajectory pair, the curve must somewhere rise quite steeply as the mass ratio approaches the integrable values of zero or unity.

smoothly over a more or less small interval ΔE. Second, distinguishing between linear and exponential separation depends heavily upon integration accuracy and upon the length of time the trajectory is integrated. Third, since each mass ratio we studied yielded (at sufficiently large energy E) a clearly "divided" energy surface on which certain trajectory pairs separated linearly while others separated exponentially, E_c depends very much on the initial conditions of the trajectory pair investigated. Finally since Fig. 3 indicates that this system is nonintegrable at large energy E for every mass ratio $m_2/m_1 \neq 0$ or 1, one expects[15] the energy surface to be "divided" no matter how small the total energy $E > 0$. Thus, mathematically speaking, there is no transition at all, there being only a smooth increase in the size of the region containing erratic or stochastic trajectories; from the physical (or computer) viewpoint, however, the transition may be regarded as occurring when the regions of erratic trajectories first become "macroscopically visible" on the energy surface or, more or less equivalently, when the exponential separation of trajectory pairs becomes sufficiently rapid to be observable using routine computer accuracy and reasonable computer integration times. Despite all these equivocations, the curve in Fig. 3 does provide, as we shall demonstrate in greater detail later, a useful dividing line below which the system exhibits primarily near-integrable behavior and above which the system exhibits primarily stochastic (nonintegrable) behavior.

We obtained the data for Fig. 3 by numerically integrating a single trajectory pair for each member of a set of increasing energy values, holding the mass ratio constant. We bounded E_c by computing the least E for which the trajectory separation was obviously exponential and the largest E below this for which it was clearly linear. We repeated this process for many mass ratios. We arbitrarily selected one member of the single trajectory pair which we integrated by first choosing a value for q_1 and then numerically setting $q_2 = \frac{2}{5} q_1$, $p_1 = \frac{1}{2} q_1$, and $p_2 = \frac{4}{7} q_1$; changing q_1 is then equivalent to changing the total energy E and, of course, we computed E for each q_1. Initial conditions for the other member of the trajectory pair were obtained by holding q_2, p_1, and p_2 constant and by then adding 10^{-6} to the original q_1 coordinate. We integrated each trajectory pair for 300 sec of differential-equation time. We then divided this 300-sec interval into three equal subintervals, and computed the average slope of the trajectory-pair separation distance D vs time for each subinterval by computing a least-squares straight-line fit to 240 equidistant points in each subinterval. At the same time, we similarly computed the average slope of $\log_{10} D$ vs time. From data similar to that shown in Figs. 1 and 2, we determined that, when the separation distance D grows linearly, the slope of D vs time had the same order of magnitude in each subinterval, for example $(10^{-5}, 10^{-5}, 10^{-5})$. On the other hand, for exponential growth, we found the slope of D vs time changed like $(10^{-5}, 10^{-4}, 10^{-3})$ or $(10^{-5}, 10^{-3}, 10^{-1})$, while the three slopes of $\log_{10} D$ vs time were then constant in order of magnitude. Finally in all calculations, the mass ratio m_2/m_1 was varied by setting $m_1 = 1$ and varying m_2; we considered only the mass-ratio interval $0 \leq m_2/m_1 \leq 1$, because Hamiltonian (1) is invariant to interchange of m_1 and m_2.

In order to present a survey of the character of system trajectories as a function of total energy E and mass ratio m_2/m_1, we now display a set of Poincaré surfaces of section. Each surface of section presents a relatively complete graphical survey of trajectory behavior at fixed E and m_2/m_1; in particular, it shows the points of intersection made by selected trajectories with a two-dimensional, cross-sectional plane cutting through the three-dimensional energy hypersurface. In regions of near-integrable behavior, most trajectories yield intersection points which line on curves[9]; erratic trajectories, on the other hand, yield a wild scatter of intersection points[9] which appear to rather uniformly cover some region of the surface-of-section plane.

Examining Fig. 3, we note that, at energy $E = 2$, Hamiltonian (1) should yield near-integrable behavior for all mass ratios. Figures 4–6 present surfaces of section at $E = 2$ for the three mass-ratio values $m_2/m_1 = 0.33$, 0.54, and 1.0; in these figures we note, as anticipated, that all the trajectories we integrated yielded a set of intersection points lying on some smooth curve. Here and in the following figures, when a trajectory yielded a set of points obviously lying on a smooth curve, the curve has been drawn in freehand. In each case studied, we have selected the (q_1, p_1) plane as our surface of section, and each curve in Figs. 4–6 gives the set of (q_1, p_1) coordinates of phase-space points on a system trajectory at which $q_2 = 0$ and $p_2 \geq 0$. The outermost, bounding curve in all surface-of-section plots is not a curve generated by a single trajectory; it represents the boundary of the intersection region between the (q_1, p_1) plane and the energy hypersurface. This bounding curve in all figures is given by

$$E = \tfrac{1}{2} p_1^2 + e^{-q_1} + e^{q_1} - 2 \,, \tag{3}$$

since $m_1 = 1$ always. Thus, at fixed energy E, the bounding curve is independent of mass ratio.

Further inspection of Fig. 3 reveals that the mass-ratio values $m_2/m_1 = 0.33$ and 0.54 should exhibit at least some erratic trajectories at $E = 7.0$; the mass ratio $m_2/m_1 = 1$, of course, yields integrable behavior at this and all other energies. Figures 7–9 verify the predictions of Fig. 3. Both Figs. 7 and 8 exhibit the "divided" energy surface mentioned earlier. Again, as discussed earlier, each curve in Figs. 7 and 8 was generated by a single trajectory, but, in addition here, the set of "random" intersection points in each figure was also generated by integrating a single trajectory, although there is a serious question (to be discussed in Sec. III) concerning computer accuracy in integrating such exponentially unstable orbits. Figures 7 and 8 make it graphically clear that linear versus exponential behavior depends strongly on trajectory-pair initial conditions, again emphasizing that Fig. 3 provides only a crude estimate for E_c. Finally, in Figs. 10–13, we present

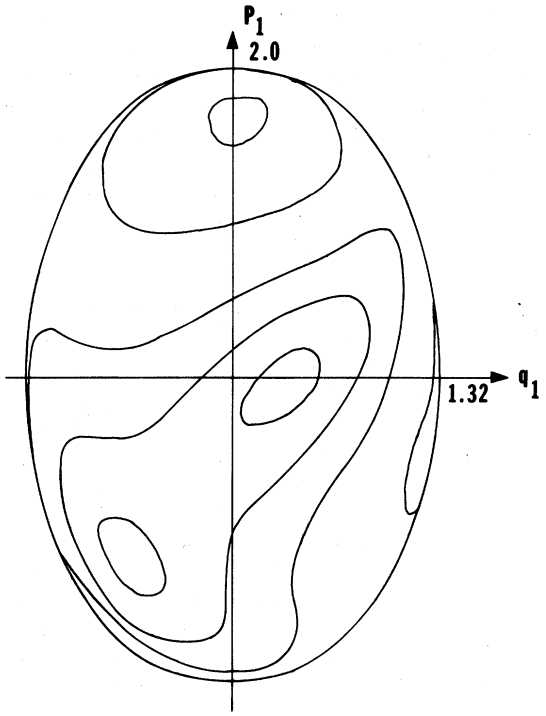

FIG. 4. Surface-of-section plot at total energy $E = 2$ for mass ratio $m_2/m_1 = 0.33$. Each curve represents the surface-of-section intersection points generated by a single trajectory. Here and in Fig. 5, all trajectories we investigated (not all are shown here) generated smooth curves; however, for reasons mentioned in the main body of this paper, we believe that at $E = 2$ this system is actually near-integrable rather than precisely integrable. Here and in all surface-of-section plots, the numbers appearing just outside the bounding curve along the q_1 and p_1 axes are the q_1 and p_1 coordinates at which the bounding curve intersects these axes.

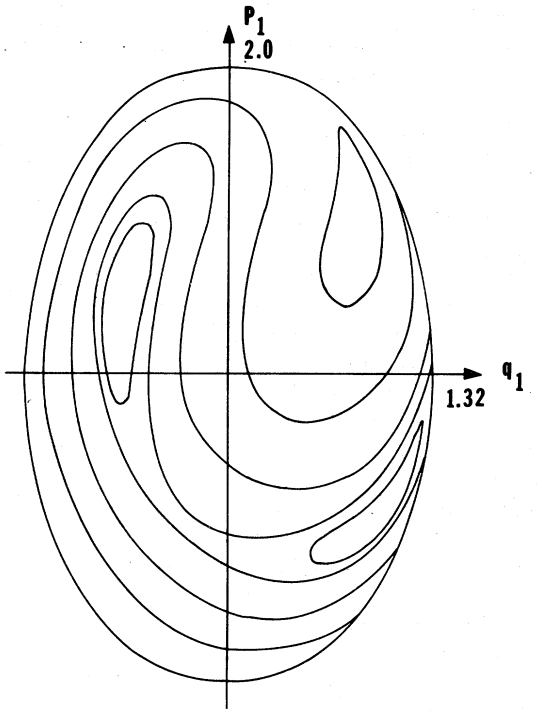

FIG. 5. Surface-of-section plot at total energy $E = 2$ for mass ratio $m_2/m_1 = 0.54$.

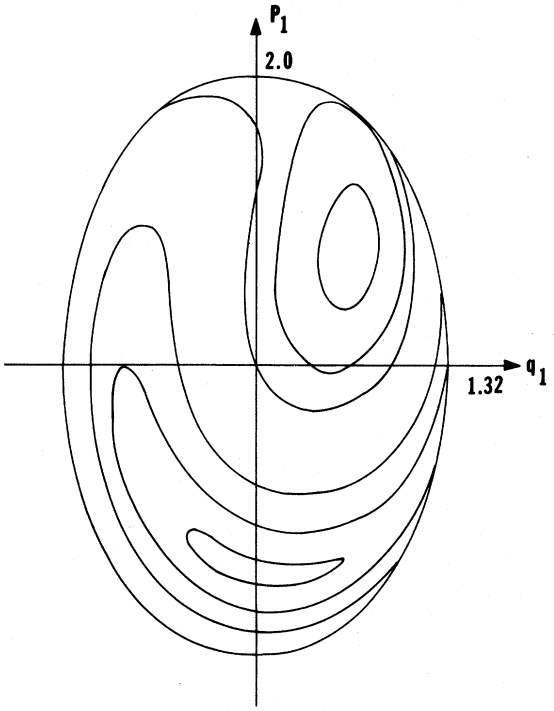

FIG. 6. Surface-of-section plot at total energy $E = 2$ for mass ratio $m_2/m_1 = 1.0$, the integrable case. Here, these directly integrated curves are in excellent agreement with those which may be calculated algebraically for this integrable case.

surfaces of section at $E=30$ for the four mass ratios $m_2/m_1=0.33$, 0.54, 0.92, and 1.0. Figures 10 and 11 show that, at this relatively large energy, the mass ratios $m_2/m_1=0.33$ and 0.54 yield erratic (or stochastic) trajectories over most of the energy hypersurface. Figure 12, at $m_2/m_1=0.92$, shows the decrease in erratic trajectories as the mass ratio tends to unity, which is the integrable case shown in Fig. 13.

III. DISCUSSION OF RESULTS

Let us open this section with a discussion of computer integration accuracy. All our numerical integrations were performed using a standard fourth-order Runge-Kutta subroutine with a fixed integration step size of 0.50 or less. All runs were performed on a UNIVAC 1108 using 16-digit double-precision arithmetic. We assured ourselves that our computer program was actually integrating the differential equations obtained from Hamiltonian (1) by comparing the directly integrated $m_1=m_2$ surfaces of section shown in Figs. 6, 9, and 13 with surfaces of section computed algebraically using the known, additional constant of the motion[2] which is available for the equal-

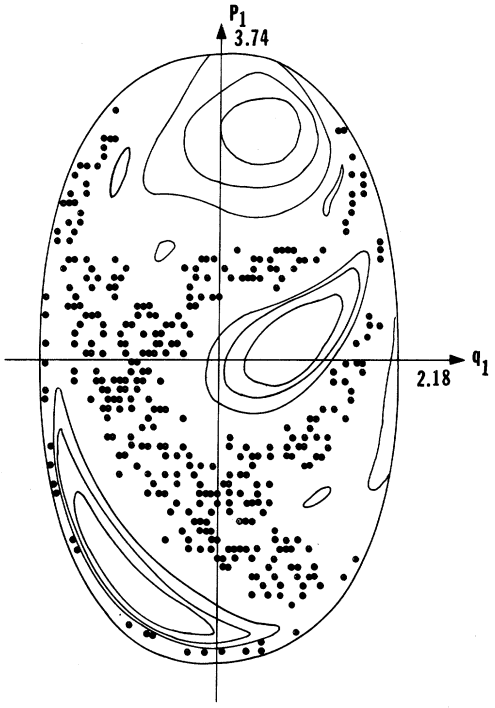

FIG. 7. Surface of section at total energy $E=7$ for mass ratio $m_2/m_1=0.33$. The set of unconnected points were generated by a single erratic trajectory. This figure presents an example of a system having a divided phase space.

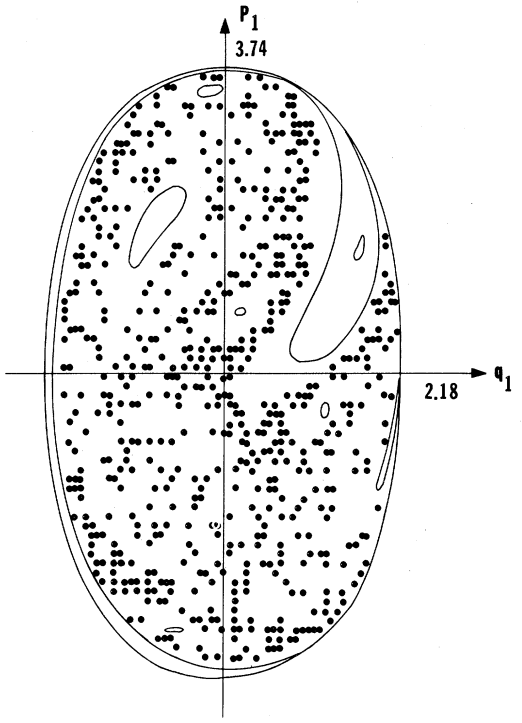

FIG. 8. Surface of section at $E=7$ for mass ratio $m_2/m_1=0.54$. The stochastic region is here even larger than that appearing in Fig. 7.

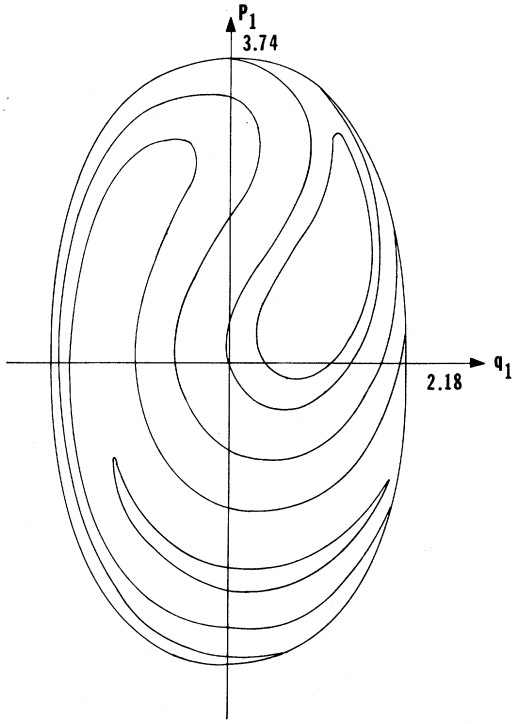

FIG. 9. Surface of section at $E=7$ for the integrable mass ratio $m_2/m_1=1.0$ presented for comparison with Figs. 7 and 8.

mass case. In addition, we numerically integrated the equal-mass case at $E=1\times10^{-5}$, obtaining the almost-harmonic surface of section shown in Fig. 14. This figure is in excellent agreement with the surface of section algebraically computed using the harmonic-oscillator approximation to the equal-mass Toda lattice. Integration accuracy was further checked by time reversing several of our longest, near-integrable trajectory integrations and regaining the initial state to at least six- or seven-digit accuracy, by noting that energy was always conserved to at least ten-digit accuracy, and by estimating error growth using data similar to that shown in Figs. 1 and 2.

With few exceptions, trajectory integrations ran for no more than 300 sec of differential-equation time. Grossly overestimating the initial error in a single trajectory integration at 10^{-14}, we see from Fig. 2 that even unstable orbits would be in error by no more than 10^{-5} after 300 sec. Consequently, Figs. 1–13, which require at most three-digit accuracy, certainly present accurate data. The exceptions are the few erratic trajectories we integrated to obtain the splatter of "random" points which appear in some surface-of-section figures. These highly unstable orbits were integrated for as much as 2000 differential-equation seconds; thus, not all of the surface-of-section points shown actually belong to a single, true orbit. However, we ran many highly accurate computer experiments to show that initially close orbits do separate exponentially when the trajectory pair is initiated anywhere within the surface-of-section region covered by the "inaccurate" splatter of dots. Moreover, in none of our calculations, no matter how long, did integration inaccuracy cause an erratic trajectory integration to yield surface-of-section points lying in a region known to contain curves. Finally, there are analytic arguments which support the belief that a truly accurate long integration of a single erratic trajectory would yield a splatter of points covering the same "erratic" surface-of-section regions shown in our figures. For all these reasons, we used an inaccurately integrated, single erratic trajectory as a particularly convenient and valid method for determining the size and shape of the

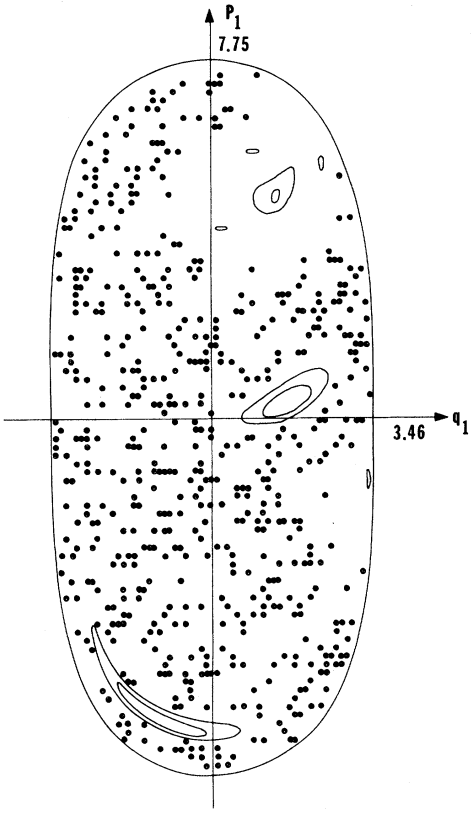

FIG. 10. Surface of section at $E=30$ for $m_2/m_1=0.33$, showing the increase in size of the stochastic region which occurs as the energy is increased.

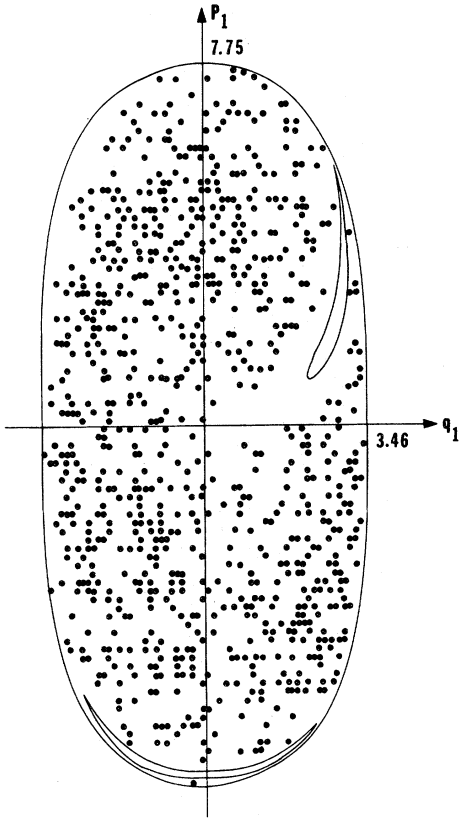

FIG. 11. Surface of section at $E=30$ for $m_2/m_1=0.54$.

"erratic" surface-of-section areas. For all the same reasons, we were content to use a computer-controlled typewriter to draw the surface-of-section points generated by these erratic orbits; this explains the horizontal and vertical order apparent in the figures.

Figures 1–13 thus present quite strong empirical evidence supporting the existence of a stochastic transition in the unequal-mass, two-particle Toda lattice. Indeed, our evidence indicates that this stochastic transition occurs for every mass ratio, excluding $m_2/m_1 = 0$ or 1. Examining Fig. 3, one notes that over a sizeable interval of mass ratios, this stochastic transition occurs at about $E_c = 2$. It is thus of interest to note that at $E = 2$ this anharmonic system is still relatively close to being harmonic in the sense that the time average of the anharmonic coupling energy is on the order of about 4% of the total energy E. Below $E = 2$, it is mathematically possible, though highly unlikely,[15] for this system to be exactly integrable instead of merely near-integrable. Certainly, computer experiments could be used to determine[16] whether or not homoclinic points[17] or hyperbolic (with re-

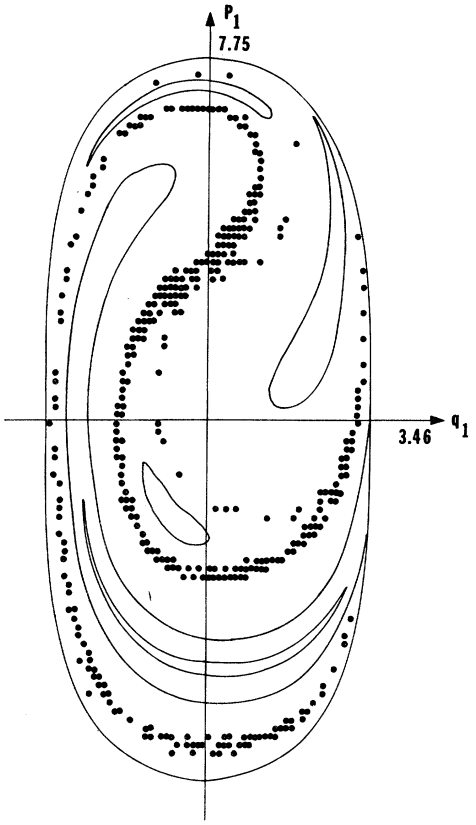

FIG. 12. Surface of section at $E = 30$ for $m_2/m_1 = 0.92$ showing that, at fixed energy, the stochastic region decreases in size as the mass ratio approaches unity.

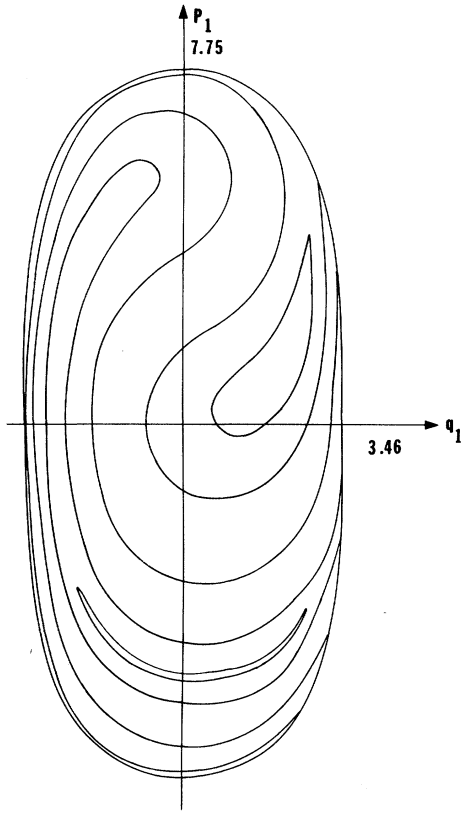

FIG. 13. Surface of section at $E = 30$ for $m_2/m_1 = 1.0$ presented for comparison with the Figs. 10–12.

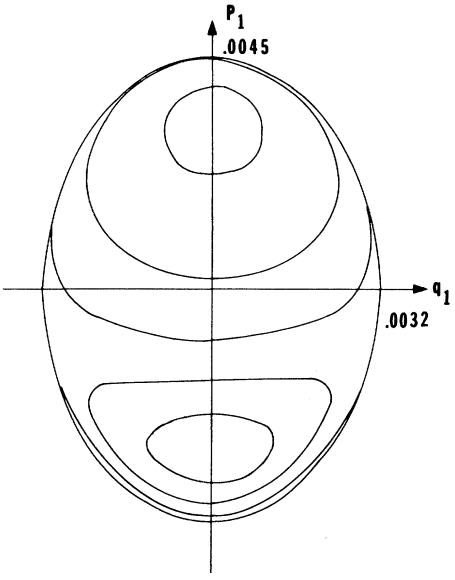

FIG. 14. Surface of section at $E = 10^{-5}$ for $m_2/m_1 = 1.0$. This surface of section differs negligibly from that of the harmonic-oscillator approximation to the equal-mass Toda lattice. The fixed points at the center of the two regions of ovals are generated by the two periodic normal modes of the harmonic system.

flection) fixed points[18] exist in the surface-of-section plots for $E = 2$, thus deciding the integrability question at least for some range of energies below $E = 2$. However, these computer experiments are so tedious and time consuming, and the probability of obtaining an unexpected answer is so small, that we could find little motivation for performing them. A question of much greater interest and difficulty,[19] which we also have not investigated here, concerns the possible existence of microscopically small, curve-bearing regions embedded in the macroscopically "erratic" regions. This latter question is worthy of investigation, since it is mathematically undecided, and since such curve-bearing regions might be of great significance for statistical mechanics.

---

*Research sponsored by the Air Force Office of Scientific Research under Grant No. AFOSR-73-2453.

[1]J. Ford, S. D. Stoddard, and J. S. Turner, Prog. Theor. Phys. 50, 1547 (1973).

[2]M. Henon, Phys. Rev. B 9, 1921 (1974); also see H. Flaschka, Phys. Rev. B 9, 1924 (1974).

[3]M. Toda, J. Phys. Soc. Jpn. 23, 501 (1967); Prog. Theor. Phys. Suppl. 45, 174 (1970).

[4]V. I. Arnold and A. Avez, *Ergodic Problems of Classical Mechanics* (Benjamin, New York, 1968), Appendix 26.

[5]A. C. Scott, F. Y. F. Chu, and D. W. McLaughlin, Proc. IEEE 61, 1443 (1973).

[6]J. Moser, Courant Institute of Mathematical Sciences report (unpublished).

[7]C. L. Siegel, Ann. Math. 42, 806 (1941); Math. Ann. 128, 144 (1954).

[8]V. I. Arnold, Russ. Math. Surv. 18, 9 (1963); also see Ref. 4, Chap. 4.

[9]M. Henon and C. Heiles, Astron. J. 69, 73 (1964).

[10]G. H. Walker and J. Ford, Phys. Rev. 188, 416 (1969).

[11]J. Ford, in *Fundamental Problems in Statistical Mechanics, III,* edited by E. G. D. Cohen (North-Holland, Amsterdam, 1975).

[12]See Ref. 4, Appendix 31; a more intuitive discussion appears in Ref. 9.

[13]B. V. Chirikov, Report No. 267, Institute of Nuclear Physics, Novosibirsk, USSR, 1969 (unpublished). An English translation of this report is available as Translation 71-40, CERN, Geneve, 1971.

[14]J. Ford, Adv. Chem. Phys. 24, 155 (1973).

[15]E. Zehnder, Comm. Pure Appl. Math. 25, 131 (1973).

[16]G. H. Lunsford and J. Ford, J. Math. Phys. 13, 700 (1972).

[17]J. M. A. Danby, Celest. Mech. 8, 273 (1973).

[18]J. Ford, in *Lecture Notes in Physics, Vol. 28: Lectures in Statistical Physics,* edited by W. C. Schieve (Springer-Verlag, New York, 1974), p. 204.

[19]G. Contopoulos, in *Recent Advances in Dynamical Astronomy,* edited by B. D. Tapley and V. Szbehely (Reidel, Dordrecht-Holland, 1973), p. 177.